Lymphatics in bone arise from pre-existing lymphatics

Marco Monroy[1], Anna L. McCarter[1], Devon Hominick[1], Nina Cassidy[1] and Michael T. Dellinger[1,2,*]

ABSTRACT

Bones do not normally have lymphatics. However, individuals with generalized lymphatic anomaly (GLA) or Gorham–Stout disease (GSD) develop ectopic lymphatics in bone. Despite growing interest in the development of tissue-specific lymphatics, the cellular origin of bone lymphatic endothelial cells (bLECs) is not known and the development of bone lymphatics has not been fully characterized. Here, we describe the development of bone lymphatics in mouse models of GLA and GSD. Through lineage-tracing experiments, we show that bLECs arise from pre-existing Prox1-positive LECs. We show that bone lymphatics develop in a stepwise manner where regional lymphatics grow, breach the periosteum and then invade bone. We also show that the development of bone lymphatics is impaired in mice that lack osteoclasts. Last, we show that rapamycin can suppress the growth of bone lymphatics in our models of GLA and GSD. In summary, we show that bLECs can arise from pre-existing LECs and that rapamycin can prevent the growth of bone lymphatics.

KEY WORDS: Gorham-Stout disease, Generalized lymphatic anomaly, VEGF-C, PIK3CA, Rapamycin

INTRODUCTION

Generalized lymphatic anomaly (GLA) and Gorham–Stout disease (GSD) are related sporadic diseases of the lymphatic system (Dellinger et al., 2014; Lala et al., 2013). Individuals with GLA or GSD develop malformed lymphatics in their soft tissues and ectopic lymphatics in bone (Dellinger et al., 2014; Lala et al., 2013). The presence of lymphatics in bone is associated with bone loss, which can cause severe deformity, paralysis and death (Dellinger et al., 2014). GLA and GSD are often difficult to treat and usually require a multidisciplinary medical team and multiple strategies. In recent years, rapamycin has become a popular treatment for GLA and GSD, and it has been reported to be effective at stabilizing or reducing signs and symptoms of disease (Adams et al., 2016; Cramer et al., 2016; Hammill et al., 2011; Ricci et al., 2019; Rodriguez-Laguna et al., 2019; Triana et al., 2017). Next-generation sequencing studies have been performed with samples from individuals with GLA and GSD to identify the genetic mutations responsible for these diseases. The hope is that this information could enable a precision medicine approach for the treatment of GLA and GSD. These studies have revealed that somatic activating mutations in *PIK3CA* can cause GLA (Rodriguez-Laguna et al., 2019). *PIK3CA* encodes p110α (a catalytic subunit of PI3K) and the

PIK3CA mutations in individuals with GLA cause hyperactivation of the PI3K/AKT/mTOR signaling pathway. A causative mutation has not been reported for GSD.

We recently developed and characterized the first mouse models of GLA and GSD. To model GLA, we used the Cre-loxP system to express an active form of *PIK3CA* (PIK3CA^{H1047R}) in lymphatic endothelial cells (LECs) in mice (Rodriguez-Laguna et al., 2019). We found that *Prox1-CreER^{T2};LSL-Pik3ca^{H1047R}* mice developed a hyperbranched network of dermal lymphatics and ectopic lymphatics in bone (Rodriguez-Laguna et al., 2019). We also found that rapamycin could prevent dermal lymphatic hyperplasia and lymphatic dysfunction in *Prox1-CreER^{T2};LSL-Pik3ca^{H1047R}* mice (Rodriguez-Laguna et al., 2019). Additionally, we found that rapamycin could attenuate dermal lymphatic hyperplasia and partially normalize lymphatic function in *Prox1-CreER^{T2};LSL-Pik3ca^{H1047R}* mice with established disease (Rodriguez-Laguna et al., 2019). To model GSD, we used the Osterix (Osx) promoter to overexpress the lymphatic growth factor vascular endothelial growth factor C (VEGFC) in bone (Hominick et al., 2018). We found that *Osx-tTA-TetO-Cre;TetO-Vegfc* mice developed lymphatics in bone and gradually lost cortical bone (Hominick et al., 2018). Loss of cortical bone is what distinguishes GSD from GLA (Lala et al., 2013). Although substantial progress has been made in our understanding of GLA and GSD, many questions still exist regarding the development of bone lymphatics. The cellular origin of bone lymphatic endothelial cells (bLECs) is not known, the stepwise development of bone lymphatics has not been fully characterized and the effect of rapamycin on the formation of bone lymphatics has not been explored. Here, we use our animal models of GLA and GSD to fill these gaps in knowledge.

RESULTS

Lineage tracing of Osx-positive cells in *Osx-tTA-TetO-Cre; TetO-Vegfc* mice

Table S1 provides a brief description of the different mouse strains used in this study. *Osx-tTA-TetO-Cre* mice express the tetracycline transactivator protein and Cre recombinase in osteoblasts, osteocytes and chondrocytes (Chen et al., 2014). To determine whether bone lymphatic endothelial cells (bLECs) originate from an Osx-positive progenitor, we performed a lineage tracing experiment with *Osx-tTA-TetO-Cre;TetO-Vegfc* mice (herein referred to as *Osx-tTA;TetO-Vegfc* mice) (Fig. 1A,B). We used the *mT/mG* reporter mouse for all of our lineage-tracing experiments. The *mT/mG* reporter allele causes Cre-positive cells and their descendants to express green fluorescent protein (GFP). It has previously been reported that cells labeled by *Lyve1-Cre* during embryonic development give rise to a subset of adult hematopoietic stem cells (HSCs) (Lee et al., 2016). HSCs are stem cells that create red blood cells, white blood cells and platelets. Although a subset of adult HSCs come from a *Lyve1-Cre*-positive progenitor, they and other hematopoietic cells in the bone marrow do not express Lyve1 (Lee et al., 2016) (Fig. S1). Because *Lyve1-Cre;mT/mG* mice have GFP-positive cells in bone, we used bones from these mice as a

[1]Division of Surgical Oncology, Department of Surgery and The Hamon Center for Therapeutic Oncology Research, UT Southwestern Medical Center, Dallas, TX 75390, USA. [2]Department of Molecular Biology and The Hamon Center for Regenerative Science and Medicine, UT Southwestern Medical Center, Dallas, TX 75390, USA.

*Author for correspondence (michael.dellinger@utsouthwestern.edu)
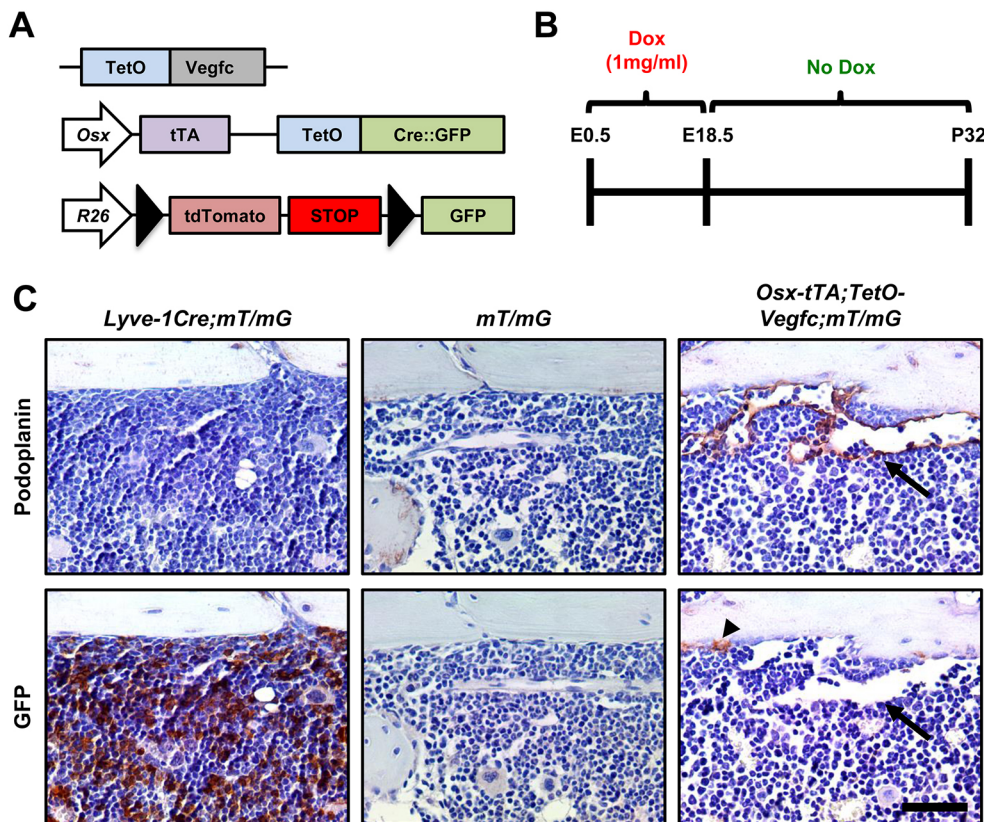
M.T.D., 0000-0002-3315-4239

DEVELOPMENT

Fig. 1. Lineage tracing of Osx-positive cells in *Osx-tTA-TetO-Cre;TetO-Vegfc; mT/mG* mice. (A) Schematics of the *TetO-Vegfc* transgene, *Osx-tTA-TetO-Cre* transgene and *mT/mG* reporter. (B) Schematic showing when *Osx-tTA-TetO-Cre;TetO-Vegfc;mT/mG* mice received doxycycline water (1 mg/ml). (C) Representative images of serial sections stained with antibodies against podoplanin and GFP. We analyzed femurs from *Lyve-1-Cre;mT/mG* mice (*n*=3 mice), *mT/mG* mice (*n*=3 mice) and *Osx-tTA-TetO-Cre;TetO-Vegfc;mT/mG* mice (*n*=3 mice). The podoplanin-positive lymphatics in *Osx-tTA-TetO-Cre;TetO-Vegfc;mT/mG* mice did not express GFP (0/24 lymphatics; 0±0, *n*=3). The arrows indicate a GFP-negative lymphatic in a femur from an *Osx-tTA-TetO-Cre;TetO-Vegfc;mT/mG* mouse. The arrowhead indicates a GFP-positive bone cell in a femur from an *Osx-tTA-TetO-Cre;TetO-Vegfc;mT/mG* mouse. Scale bar: 50 μm.

positive control for immunostaining for GFP. *mT/mG* mice do not express GFP and were used as a negative control for immunostaining for GFP. We found that femurs from *Lyve1-Cre; mT/mG* mice contained numerous GFP-positive cells, whereas femurs from *mT/mG* mice did not (Fig. 1C). Importantly, the podoplanin-positive lymphatics in the femurs of *Osx-tTA;TetO-Vegfc;mT/mG* mice did not express GFP (Fig. 1C). We confirmed that lymphatics in the femurs of *Osx-tTA;TetO-Vegfc;mT/mG* mice did not express GFP by staining for Lyve1 and GFP (Fig. S2). These results suggest that bLECs in *Osx-tTA;TetO-Vegfc* mice do not originate from an Osx-positive progenitor. Although lymphatics in the bones of *Osx-tTA;TetO-Vegfc;mT/mG* mice did not express GFP, bone cells in these mice expressed GFP in a salt and pepper fashion (Fig. 1C; Fig. S2). This is consistent with other reports showing that bone cells are labeled by the *Osx-tTA-TetO-Cre* allele (Chen et al., 2014; Rodda and McMahon, 2006).

Prox1-CreER^{T2} mice do not exhibit Cre activity in bone

We then set out to determine whether bLECs originate from pre-existing Prox1-positive LECs. First, we performed a lineage tracing experiment to determine whether *Prox1-CreER^{T2}* mice exhibit Cre activity in bone. *Prox1-CreER^{T2};mT/mG* mice were injected with tamoxifen on postnatal day (P) 21, P23, P25 and P27, and femurs were collected on P55 (Fig. 2A,B). Femurs from *Lyve1-Cre;mT/mG* mice and *mT/mG* mice were included as controls for immunostaining for GFP. We examined GFP expression by cells in the marrow cavity, on the surface of the bone, in cortical bone and in the periosseous connective tissue (Fig. 2C). Numerous GFP-positive cells were present in the marrow cavity of *Lyve1-Cre;mT/mG* mice (Fig. 2D). However, cells on the surface of the bone (osteoblasts) and in cortical bone (osteocytes) did not express GFP (Fig. 2E,F). *mT/mG* mice and *Prox1-CreER^{T2};mT/mG* mice did not

have GFP-positive cells in the marrow cavity, on the surface of the bone or in cortical bone (Fig. 2H-N). These results show that *Prox1-CreER^{T2}* mice do not exhibit Cre activity in bone. However, *Prox1-CreER^{T2};mT/mG* mice had numerous GFP-positive lymphatics in their periosseous connective tissue (Fig. 2O and Fig. S3).

Next, we examined the leakiness of Cre activity in *Prox1-CreER^{T2}* mice. We examined GFP expression by lymphatics in ear skin samples from *Prox1-CreER^{T2};mT/mG* mice that received tamoxifen (P21, P23, P25 and P27) and *Prox1-CreER^{T2};mT/mG* mice that did not receive tamoxifen. Ear skin samples from *Lyve1-Cre;mT/mG* mice and *mT/mG* mice were included as controls for immunostaining for GFP. GFP-positive lymphatics were present in ear skin samples from *Lyve1-Cre;mT/mG* mice and *Prox1-CreER^{T2};mT/mG* mice that received tamoxifen (Fig. S4). GFP was not present in ear skin samples from *mT/mG* mice or *Prox1-CreER^{T2};mT/mG* mice that did not receive tamoxifen (Fig. S4). These results show that *Prox1-CreER^{T2}* mice do not exhibit Cre activity in the absence of tamoxifen and that our tamoxifen administration scheme effectively induces Cre-mediated recombination in LECs.

We then performed a pulse-chase experiment to determine how long it takes for the effect of tamoxifen on CreER^{T2} localization to wear off in *Prox1-CreER^{T2}* mice. *Prox1-CreER^{T2}* mice were injected with tamoxifen on P21, P23, P25 and P27, and tissues were collected on P28, P41 and P55 (Fig. 3A). We assessed CreER^{T2} localization by immunostaining with an antibody that detects the ER region of the CreER^{T2} protein. We were unable to assess the effect of tamoxifen on CreER^{T2} localization in bone because *Prox1-CreER^{T2}* mice do not exhibit Cre activity in bone. We decided to analyze livers from *Prox-1CreER^{T2}* mice because Prox1 is expressed by hepatocytes and because the size and shape of
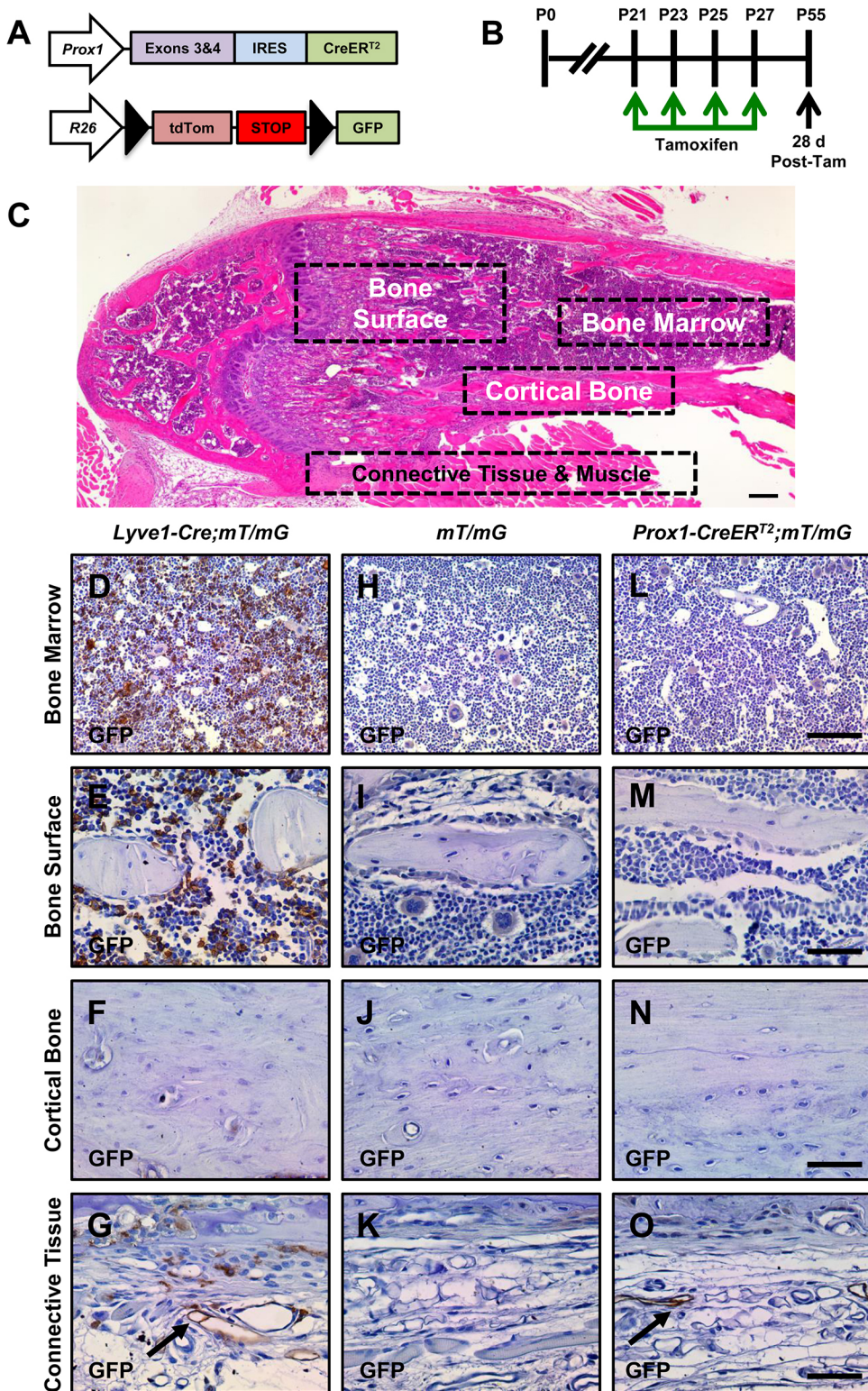
Fig. 2. *Prox1-CreER^T2* mice do not exhibit Cre activity in bone. (A) Schematics of the *Prox1-CreER^T2* construct and *mT/mG* reporter. (B) Schematic showing when *Prox1-CreER^T2;mT/mG* mice were injected with tamoxifen (2 mg; i.p.). (C) Low-magnification image of an Hematoxylin and Eosin-stained femur that shows the different areas analyzed in *Lyve-1Cre;mT/mG*, *mT/mG* and *Prox1-CreER^T2;mT/mG* mice. (D-O) Representative images of femurs stained with an anti-GFP antibody. Femurs were analyzed from *Lyve-1Cre;mT/mG* mice (positive control; *n*=3 mice), *mT/mG* mice (negative control; *n*=3 mice) and *Prox1-CreER^T2;mT/mG* mice (*n*=3 mice). GFP was not expressed by cells in the marrow cavity, in cortical bone or on the surface of the bone (osteoblasts and osteoclasts) in *Prox1-CreER^T2;mT/mG* mice. The arrows in G and O indicate GFP-positive lymphatics in periosseous connective tissue. Scale bars: 200 μm in C; 100 μm in L (for D,H,L); 50 μm in M-O.

hepatocytes would allow us to reliably distinguish between cytoplasmic and nuclear localization of the CreER^T2 protein. We found that CreER^T2 was localized to the nucleus on P28 but not on P41 or P55 (Fig. 3B-F). These results suggest that the effects of tamoxifen on CreER^T2 localization wear off sometime between P28 and P41. However, the kinetics of tamoxifen distribution and retention may be different in different tissues.

Lineage tracing of Prox1-positive cells in *Osx-tTA;TetO-Vegfc* mice

After we characterized Cre activity in *Prox1-CreER^T2* mice, we performed a lineage-tracing experiment to determine whether bLECs arise from pre-existing LECs. First, we performed several pilot studies to determine the conditions that would cause *Osx-tTA; TetO-Vegfc* mice to develop lymphatics in bone after P41 (the end of
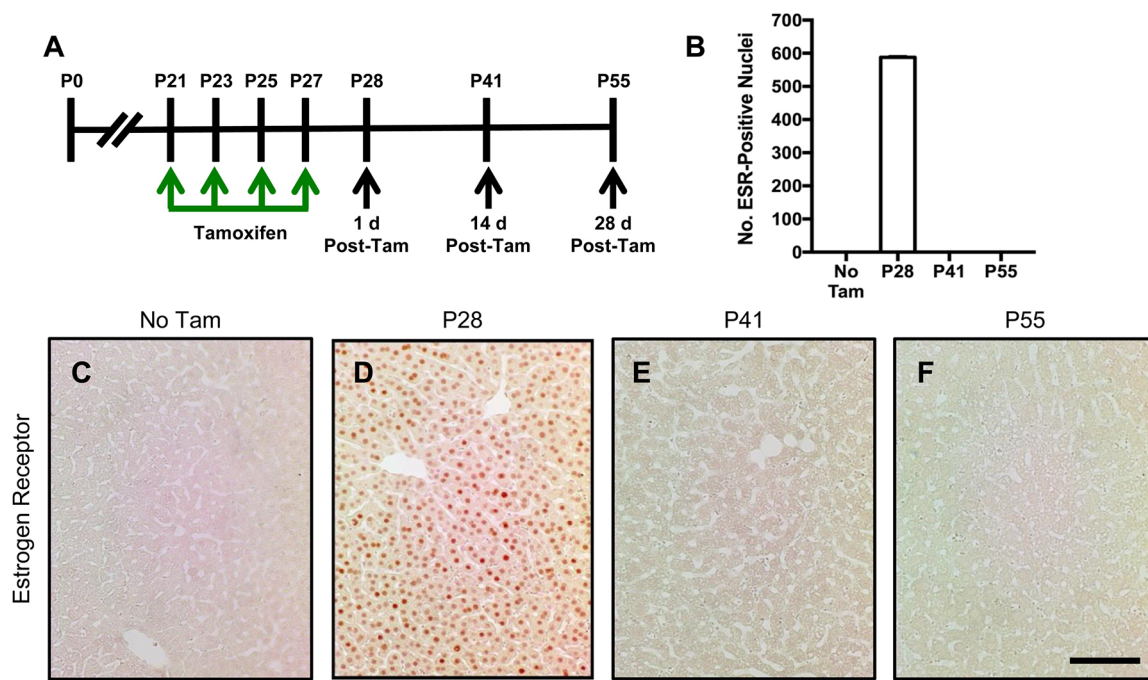
Fig. 3. Localization of Cre recombinase in *Prox1-CreER^T2* mice. (A) Schematic showing when *Prox1-CreER^T2* mice were injected with tamoxifen (2 mg; i.p.). (B) Graph showing the number of estrogen receptor-positive nuclei in livers from *Prox1-CreER^T2* mice that did not receive tamoxifen (0±0, *n*=3) and from *Prox1-CreER^T2* mice 1 day (588±3.22, *n*=3), 14 days (0±0, *n*=3), and 28 days (0±0, *n*=3) after they received their last pulse of tamoxifen. (C-F) Representative images of livers stained with an anti-estrogen receptor antibody. CreER^T2 moved out of the nucleus sometime between P28 and P41. Data are mean±s.e.m. Scale bar: 100 μm.

the tamoxifen washout period). We found that *Osx-tTA;TetO-Vegfc* mice developed lymphatics in bone after P41 if we gave them doxycycline water (0.2 mg/ml) from embryonic day (E) 0.5 to P21.

Next, we gave *Osx-tTA;TetO-Vegfc;Prox1-CreER^T2;mT/mG* mice doxycycline water (0.2 mg/ml) from E0.5 to P21 and then injected them with tamoxifen on P21, P23, P25 and P27 (Fig. 4A,B). We collected bones on P45 and P65, and stained them with antibodies against GFP and Lyve1. Bones collected on P45 contained numerous GFP-positive and Lyve1-negative bone cells (Fig. 4C). We have previously shown that bone cells are labeled by *Osx-tTA-TetO-Cre* but not *Prox1-CreER^T2* (Fig. S2, Fig. 2). Bones collected on P45 did not have lymphatics (0±0, *n*=4 mice; Fig. 4C,D). In contrast, bones collected on P65 contained Lyve1-positive lymphatics (Fig. 4C,D). Approximately 85% of the lymphatics expressed GFP (85.98±3.227, *n*=4 mice). Importantly, these lymphatics developed after the tamoxifen washout period (P28-P41).

Stepwise development of bone lymphatics

Next, we set out to characterize the stepwise development of bone lymphatics. We have previously analyzed the development of bone lymphatics in femurs from *Osx-tTA;TetO-Vegfc* mice (Hominick et al., 2018). We reported that we could detect lymphatics in cortical bone before we could detect them in the marrow cavity (Hominick et al., 2018). It is standard practice to strip femurs free of connective tissue before fixing and decalcifying them. Because we did that in our previous study, we were not able to characterize the initial stages of development of bone lymphatics. To fill this gap in knowledge, we analyzed tissue sections where we kept the periosseous muscle tissue and periosteum intact. The periosteum is the layer of tissue that covers the outside surface of bones. We collected ribs from *TetO-Vegfc* and *Osx-tTA;TetO-Vegfc* mice on P20, P24, P28 and P32, and stained tissue cross-sections using an antibody against Lyve1 (Fig. 5A). We then surveyed the periosseous muscle, cortical

bone and marrow cavity for lymphatics (Fig. 5B). Lymphatics in *TetO-Vegfc* mice were restricted to the intercostal muscle tissue and they never traversed the periosteum (Fig. 5C-H, Table S2). In contrast, regional lymphatics in *Osx-tTA;TetO-Vegfc* mice grew, breached the periosteum, separated the periosteum from bone and then gradually invaded bone (Fig. 5C-H, Table S2).

Osteoclasts are associated with lymphatics invading bone and the development of bone lymphatics is impaired in osteoclast-deficient mice

Next, we characterized the invasion of bone by lymphatics. Osteoclasts are large multinucleated cells that degrade bone. Although we have previously reported that *Osx-tTA;TetO-Vegfc* mice have more osteoclasts than control mice, we did not examine the relationship between osteoclasts and lymphatics in bone (Hominick et al., 2018). To determine whether osteoclasts were associated with lymphatics invading bone, we stained serial sections of bone from *Osx-tTA;TetO-Vegfc* mice for TRAP activity (marker of osteoclasts) and Lyve1. We found that osteoclasts were closely associated with invading lymphatics (Fig. S5).

Colony-stimulating factor 1 (Csf1) is a secreted protein that is required for the development of osteoclasts (Dai et al., 2002). To determine whether osteoclasts are required for the development of bone lymphatics, we used a genetic approach to suppress osteoclast development in *Osx-tTA;TetO-Vegfc* mice. We found that *Osx-tTA;TetO-Vegfc;Csf1^mut/mut* mice had denser bones and significantly fewer osteoclasts than *Osx-tTA;TetO-Vegfc;Csf1^wt/mut* mice (Fig. 6A-F). The density of lymphatics in the intercostal muscle tissue was not significantly different between *Osx-tTA;TetO-Vegfc;Csf1^mut/mut* and *Osx-tTA;TetO-Vegfc;Csf1^wt/mut* mice (Fig. 6G,H). This result shows that periosseous lymphangiogenesis occurs in *Osx-tTA;TetO-Vegfc;Csf1^mut/mut* and *Osx-tTA;TetO-Vegfc;Csf1^wt/mut* mice. In contrast to *Osx-tTA;TetO-Vegfc;Csf1^wt/mut* mice, the
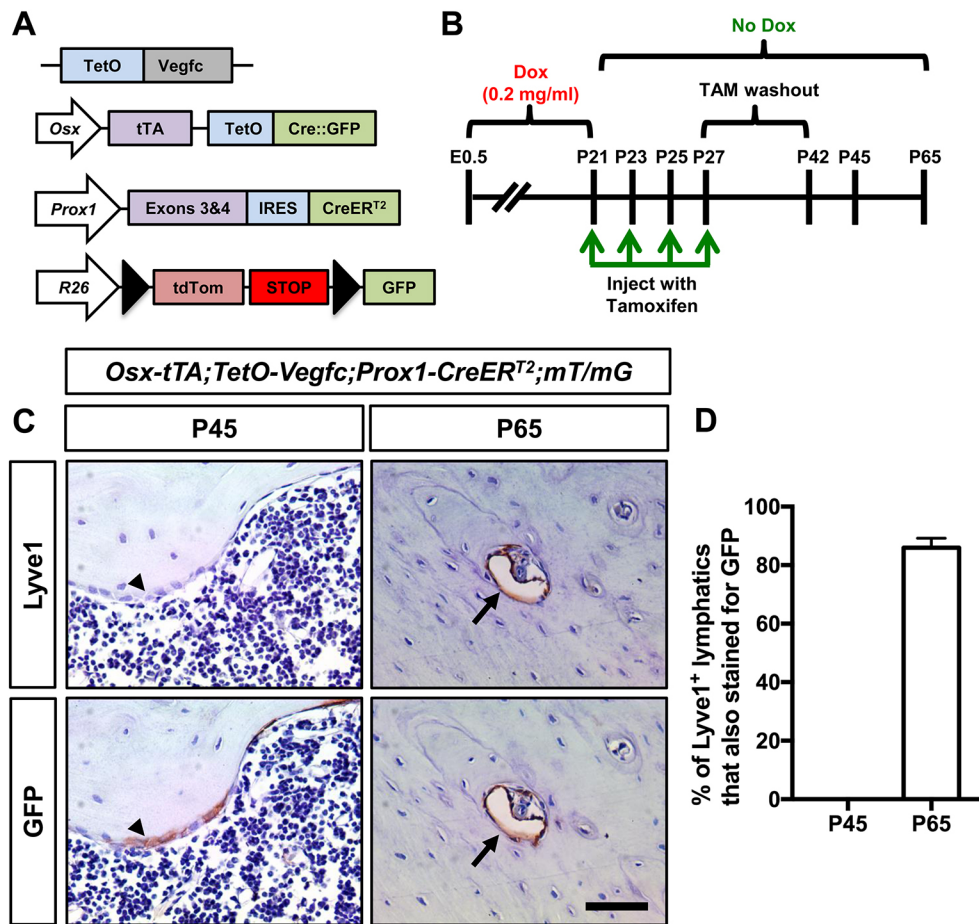
Fig. 4. Lineage tracing of Prox1-positive cells in *Osx-tTA;TetO-Vegfc* mice. (A) Schematics of the *TetO-Vegfc* transgene, *Osx-tTA-TetO-Cre* transgene, *Prox1-CreER^{T2}* construct and *mT/mG* reporter. (B) Schematic showing when *Osx-tTA;TetO-Vegfc;Prox1-CreER^{T2}; mT/mG* mice received doxycycline water (0.2 mg/ml) and tamoxifen (2 mg; i.p.). (C) Representative images of serial sections stained with antibodies against Lyve1 and GFP. Femurs collected on P45 (*n*=4 mice) did not contain lymphatics. The arrowheads indicate Lyve1-negative GFP-positive osteoblasts on the bone surface. Femurs collected on P65 were filled with lymphatics (*n*=4 mice). The arrows indicate a Lyve1-positive-GFP-positive lymphatic in bone. (D) Approximately 85% of the Lyve1-positive lymphatics in P65 mice expressed GFP (85.98±3.227, *n*=4). P45 mice did not have lymphatics in bone (0±0, *n*=4). Data are mean±s.e.m. Scale bar: 50 μm.

cortical bone and bone marrow in *Osx-tTA;TetO-Vegfc;Csf1^{mut/mut}* mice was almost completely devoid of lymphatics (Fig. 6G,I,J).

Lineage tracing of Prox1-positive cells in *Prox1-CreER^{T2}; LSL-Pik3ca^{H1047R}* mice

We have previously shown that *Prox1-CreER^{T2};LSL-Pik3ca^{H1047R}* mice develop ectopic lymphatics in bone (Rodriguez-Laguna et al., 2019). Because we did not include a lineage reporter in our previous animal study (Rodriguez-Laguna et al., 2019), the origin of bLECs in *Prox1-CreER^{T2};LSL-Pik3ca^{H1047R}* mice was unclear. Therefore, we performed a lineage-tracing study with *Prox1-CreER^{T2};LSL-Pik3ca^{H1047R}* mice to determine whether bLECs in these mice come from pre-existing LECs. The tamoxifen injection schedule used for *Prox1-CreER^{T2};LSL-Pik3ca^{H1047R}* mice is different from the schedule used for *Osx-tTA;TetO-Vegfc;Prox1-CreER^{T2};mT/mG* mice. Therefore, we performed another pulse-chase experiment to determine how long it takes for the effect of tamoxifen on CreER^{T2} localization to wear off in *Prox1-CreER^{T2}* mice. *Prox1-CreER^{T2}* mice were injected with tamoxifen on P31, P33, P35, P39 and P42, and livers were collected on either P43 or P70 (Fig. 7A). As before, we assessed the localization of CreER^{T2} by immunostaining for ER. CreER^{T2} was localized to the nucleus on P43 but not on P70 (Fig. 7B-E). These results suggest that the effects of tamoxifen on CreER^{T2} localization wear off sometime between P43 and P70.

Next, we performed a lineage-tracing experiment with *Prox1-CreER^{T2};LSL-Pik3ca^{H1047R};mT/mG* mice to determine whether bLECs originate from pre-existing LECs. *Prox1-CreER^{T2};LSL-Pik3ca^{H1047R};mT/mG* mice were injected with tamoxifen on P31, P33, P35, P39 and P42 to label LECs, and femurs were collected

from mice on either P43, P70 or P98 (Fig. 7F,G). Femurs collected on P43 and P70 did not contain lymphatics (Fig. 7H,I). However, femurs collected on P98 contained lymphatics and ∼65% of the lymphatics expressed GFP (66.7±33.3, *n*=3) (Fig. 7H,I). Importantly, these lymphatics developed after the tamoxifen washout period (P43-P70).

Rapamycin suppresses the development of bone lymphatics in *Osx-tTA;TetO-Vegfc* mice

Rapamycin is an FDA-approved mTOR inhibitor that is used to treat GSD and GLA. To determine whether rapamycin could suppress the development of bone lymphatics, we treated *Osx-tTA;TetO-Vegfc* mice with rapamycin (Fig. 8A). We started to treat *Osx-tTA;TetO-Vegfc* mice with vehicle or rapamycin when they were 21 days old. We have previously shown that *Osx-tTA;TetO-Vegfc* mice do not have lymphatics in bone when they are 21 days old (Hominick et al., 2018). We collected femurs from vehicle and rapamycin-treated mice when they were 35 days old. We found that rapamycin-treated mice had significantly fewer bone lymphatics than vehicle-treated mice (Fig. 8B-D). Additionally, cortical bone porosity was lower in rapamycin-treated mice than in vehicle-treated mice (Fig. 8E-G). These results show that rapamycin can suppress the development of bone lymphatics and bone loss in *Osx-tTA;TetO-Vegfc* mice.

Rapamycin suppresses the growth of PIK3CA-mutant LECs and the development of bone lymphatics in *Prox1-CreER^{T2}; LSL-Pik3ca^{H1047R}* mice

We then set out to characterize the effect of rapamycin on PIK3CA-mutant LECs. We obtained LECs from an individual who was
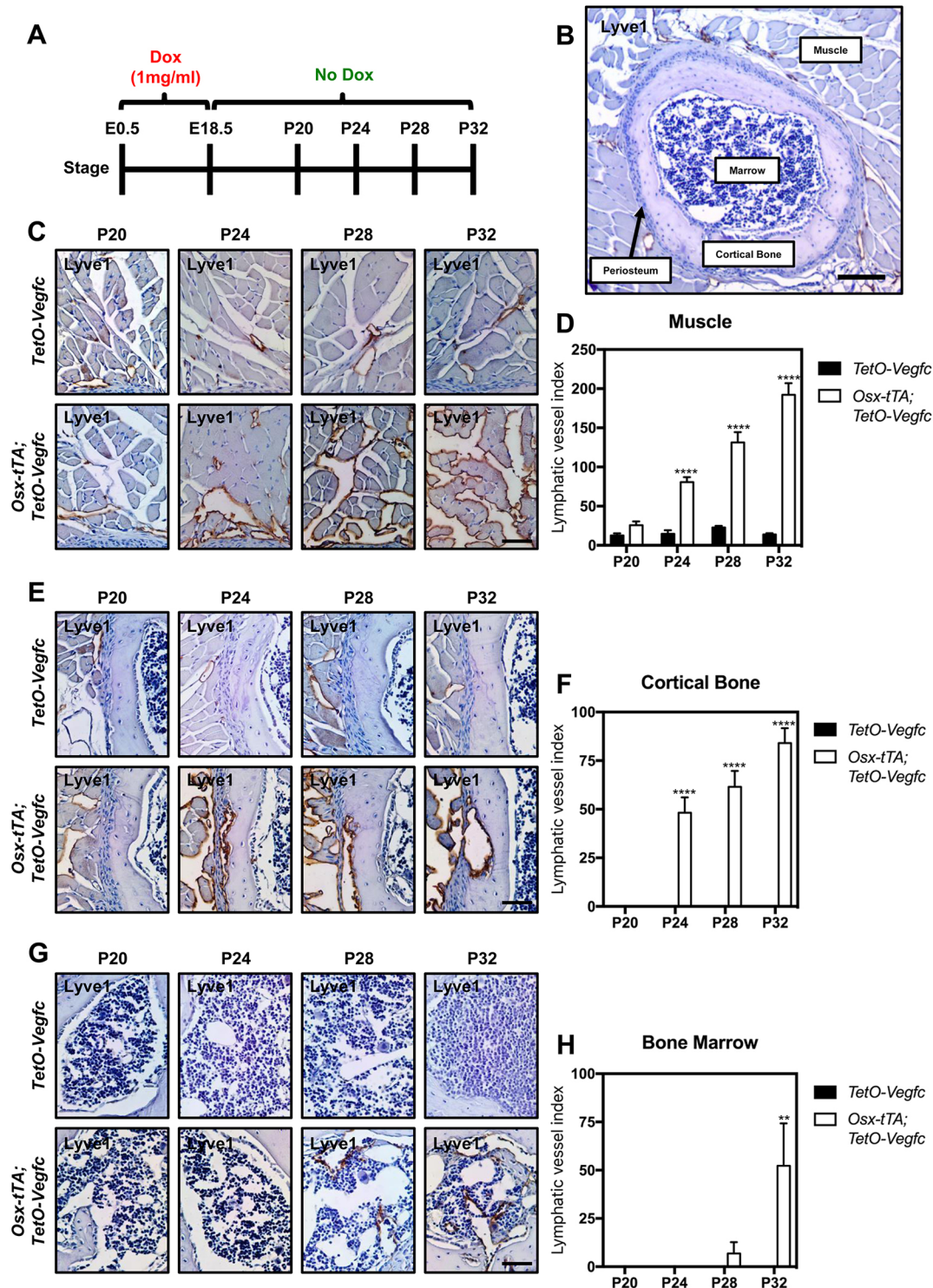
Fig. 5. Stepwise development of bone lymphatics. (A) Schematic showing when mice received doxycycline water (1 mg/ml). (B) Low-magnification image that shows periosseous muscle, the periosteum, cortical bone and bone marrow. These regions were imaged in *TetO-Vegfc* and *Osx-tTA-TetO-Vegfc* mice. (C) Images of Lyve-1-positive lymphatics in intercostal muscle tissue in *TetO-Vegfc* and *Osx-tTA;TetO-Vegfc* mice. (D) Lymphatic vessel index values for muscle in P20 (12.5±2.754, *n*=3), P24 (14.6±4.581, *n*=5), P28 (22.8±2.177, *n*=5) and P32 (13.79±1.786, *n*=7) *TetO-Vegfc* mice. Lymphatic vessel index values for muscle in P20 (25.83±4.604, *n*=3), P24 (80.8±6.176, *n*=5), P28 (131.3±13.23, *n*=6) and P32 (192.1±14.86, *n*=4) *Osx-tTA;TetO-Vegfc* mice. (E) Images of Lyve-1-positive lymphatics in cortical bone in *TetO-Vegfc* and *Osx-tTA;TetO-Vegfc* mice. (F) Lymphatic vessel index values for cortical bone in P20 (0±0, *n*=3), P24 (0±0, *n*=5), P28 (0±0, *n*=5) and P32 (0±0, *n*=7) *TetO-Vegfc* mice. Lymphatic vessel index values for cortical bone in P20 (0±0, *n*=3), P24 (48.2±7.96, *n*=5), P28 (61.5±8.172, *n*=5) and P32 (84±7.72, *n*=4) *Osx-tTA;TetO-Vegfc* mice. (G) Images of Lyve-1-positive lymphatics in bone marrow in *TetO-Vegfc* and *Osx-tTA;TetO-Vegfc* mice. (H) Lymphatic vessel index values for bone marrow in P20 (0±0, *n*=3), P24 (0±0, *n*=5), P28 (0±0, *n*=5) and P32 (0±0, *n*=7) *TetO-Vegfc* mice. Lymphatic vessel index values for bone marrow in P20 (0±0, *n*=3), P24 (0±0, *n*=5), P28 (6.9±5.84, *n*=5) and P32 (52.25±22.01, *n*=4) *Osx-tTA;TetO-Vegfc* mice. Data are mean±s.e.m. ****P<0.0001, **P<0.01; unpaired Student's *t*-test. For each timepoint, *TetO-Vegfc* mice were compared with *Osx-tTA;TetO-Vegfc* mice. Scale bars: 50 μm.
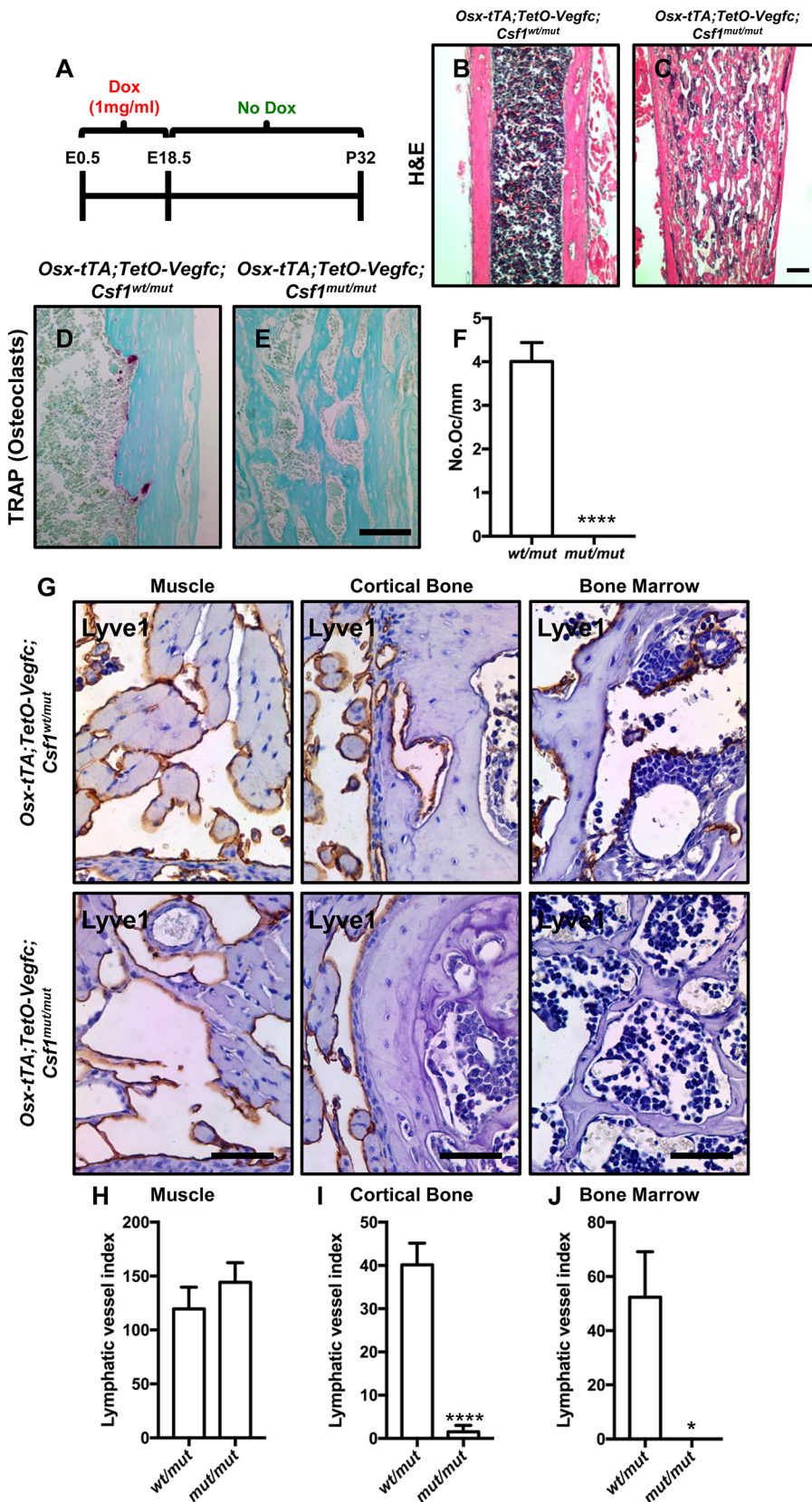
Fig. 6. The development of bone lymphatics is impaired in osteoclast-deficient mice.
(A) Schematic showing when mice received doxycycline water (1 mg/ml). (B,C) Images of Hematoxylin and Eosin-stained femur sections. *Osx-tTA;TetO-Vegfc;Csf1^{mut/mut}* mice (C) had more bone than *Osx-tTA;TetO-Vegfc;Csf1^{wt/mut}* mice (B). Scale bar: 200 μm. (D,E) Images of TRAP-stained femurs from *Osx-tTA;TetO-Vegfc;Csf1^{wt/mut}* and *Osx-tTA;TetO-Vegfc;Csf1^{mut/mut}* mice. (F) *Osx-tTA; TetO-Vegfc;Csf1^{wt/mut}* mice (4.01±0.433, $n=4$) had significantly more osteoclasts per mm of bone surface than *Osx-tTA;TetO-Vegfc;Csf1^{mut/mut}* mice (0±0, $n=4$). (G) Images of rib sections stained with an anti-Lyve1 antibody. (H) The lymphatic vessel index values for muscle were not significantly different between *Osx-tTA;TetO-Vegfc;Csf1^{wt/mut}* (119.6±20.14, $n=4$) and *Osx-tTA;TetO-Vegfc; Csf1^{mut/mut}* mice (144.3±18.17, $n=4$). (I) The lymphatic vessel index values for cortical bone were significantly different between *Osx-tTA;TetO-Vegfc;Csf1^{wt/mut}* (40.13±5.026, $n=4$) and *Osx-tTA; TetO-Vegfc;Csf1^{mut/mut}* mice (1.5±1.5, $n=4$). (J) The lymphatic vessel index values for bone marrow were significantly different between *Osx-tTA;TetO-Vegfc;Csf1^{wt/mut}* (52.38±16.8, $n=4$) and *Osx-tTA;TetO-Vegfc;Csf1^{mut/mut}* mice (0±0, $n=4$). Data are mean±s.e.m. ****$P<0.001$, *$P<0.05$; unpaired Student's *t*-test. Scale bars: 50 μm.

reported to have a somatic activating mutation in *PIK3CA* (PIK3CA^{H1047L}-LECs) and a germline mutation in *PIK3R3* (Boscolo et al., 2015). We confirmed the identity of the cells by immunostaining for PROX1 and the mutation status of the cells by Sanger sequencing (Fig. 9A-F). We found that PIK3CA^{H1047L}-LECs formed irregular vessels in *in vitro* lymphangiogenesis assays (Fig. 9G-J). We also found that PI3K/AKT/mTORC1 signaling was greater in PIK3CA^{H1047L}-LECs than in wild-type LECs, and that
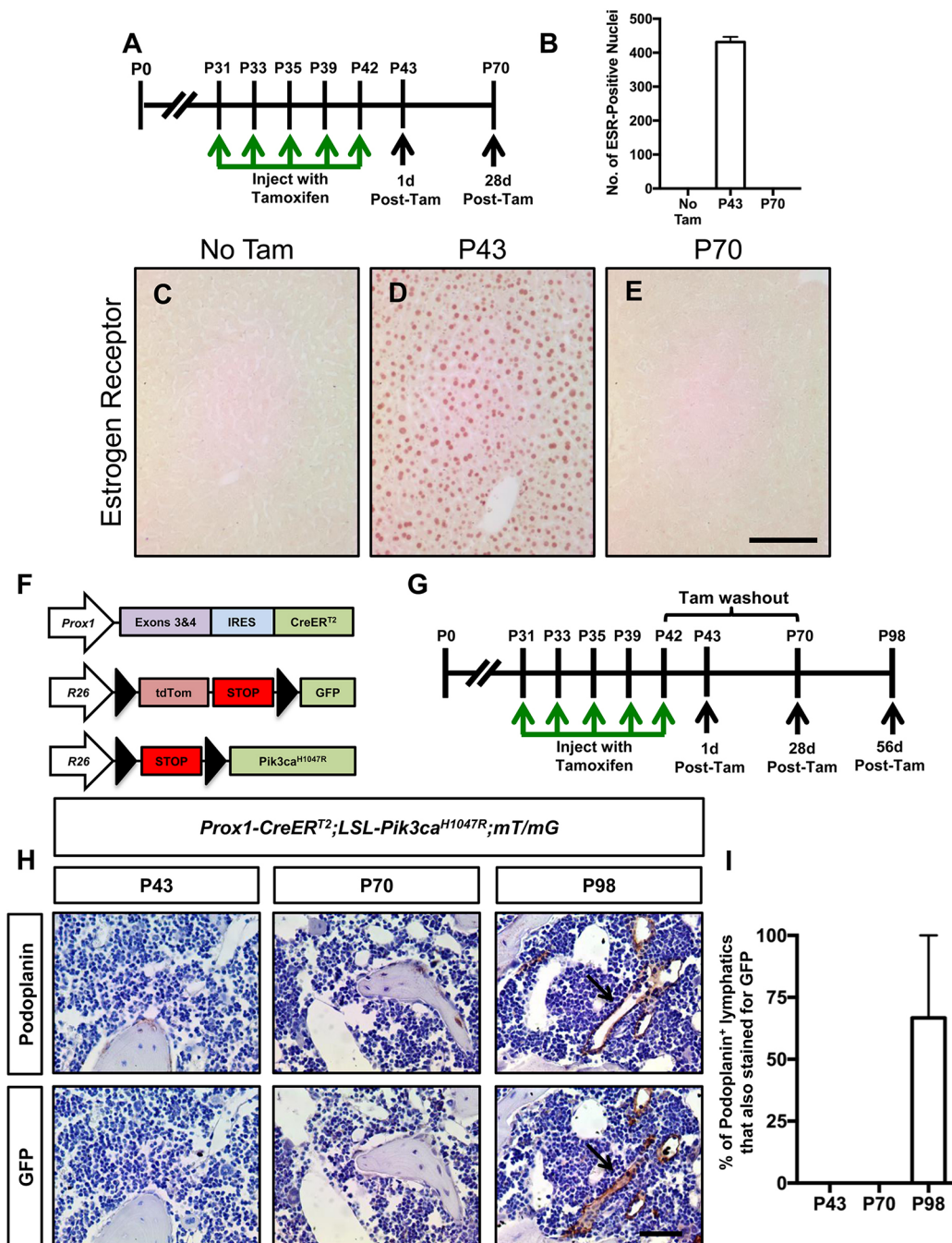
Fig. 7. Lineage tracing of Prox1-positive cells in *Prox1-CreER^T2;LSL-Pik3ca^H1047R* mice. (A) Schematic showing when *Prox1-CreER^T2* mice were injected with tamoxifen (2 mg; i.p.). (B) Graph showing the number of estrogen receptor-positive nuclei in livers from *Prox1-CreER^T2* mice that did not receive tamoxifen (0±0, *n*=3), *Prox1-CreER^T2* mice 1 day after they received their last pulse of tamoxifen (431.3±15.21, *n*=3) and *Prox1-CreER^T2* mice 28 days after they received their last pulse of tamoxifen (0±0, *n*=4). (C-E) Representative images of livers stained using an anti-estrogen receptor antibody. CreER^T2 moved out of the nucleus within 4 weeks of mice having received their last pulse of tamoxifen. Scale bar: 100 µm. (F) Schematics of the *Prox1-CreER^T2* allele, the *LSL-Pik3ca^H1047R* allele and *mT/mG* reporter. (G) Schematic showing when *Prox1-CreER^T2;LSL-Pik3ca^H1047R;mT/mG* mice were injected with tamoxifen (2 mg; i.p.). (H) Representative images of serial sections stained with antibodies against podoplanin and GFP. Lymphatics were not present in femurs collected from *Prox1-CreER^T2;LSL-Pik3ca^H1047R;mT/mG* mice on P43 (*n*=5 mice) or P70 (*n*=7 mice). Lymphatics were present in three out of 6 mice on P98. Arrows indicate GFP-positive lymphatics. Scale bar: 50 µm. (I) Approximately 65% of the lymphatics in P98 bones expressed GFP (66.7±33.3, *n*=3). Lymphatics were not present in bones on P43 (0±0, *n*=5 mice) or P70 (0±0, *n*=7). Data are mean±s.e.m.

rapamycin could suppress mTORC1 signaling and the growth of PIK3CA^H1047L-LECs and wild-type LECs (Fig. 9K-M). These results are consistent with other reports that rapamycin suppresses the growth of *PIK3CA*-mutant LECs (Blesinger et al., 2018; Boscolo et al., 2015; Osborn et al., 2015).

We have previously shown that rapamycin could prevent dermal lymphatic hyperplasia in *Prox1-CreER^T2;LSL-Pik3ca^H1047R* mice (Rodriguez-Laguna et al., 2019). We did not characterize the effect of rapamycin on the development of bone lymphatics in our previous study (Rodriguez-Laguna et al., 2019). Therefore, we set
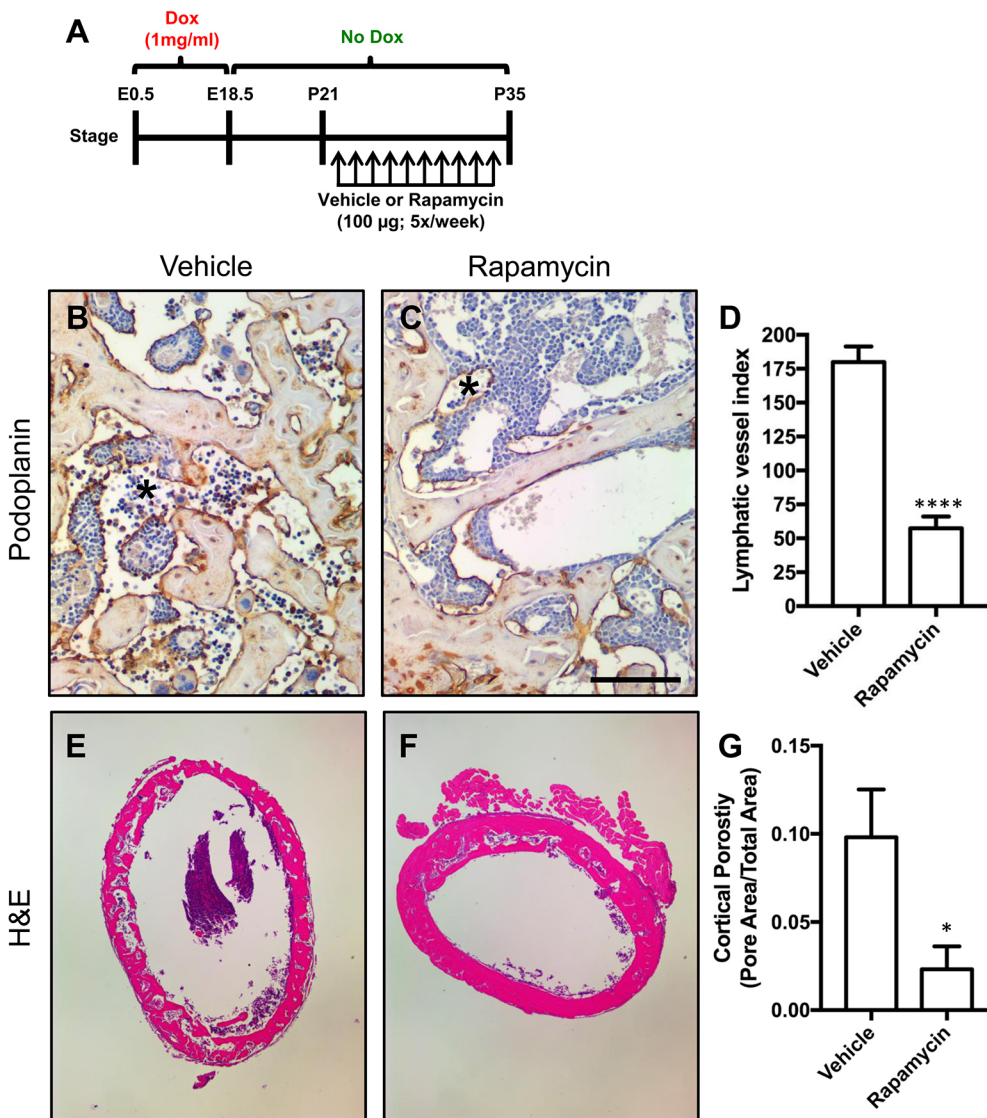
Fig. 8. Rapamycin suppresses the development of bone lymphatics in *Osx-tTA;TetO-Vegfc* mice.
(A) Schematic showing when *Osx-tTA; TetO-Vegfc* mice received doxycycline water (1 mg/ml). *Osx-tTA;TetO-Vegfc* mice were treated with vehicle or rapamycin (100 μg; 5×/week; i.p.) from P21 to P35. (B,C) Representative images of femurs stained using an anti-podoplanin antibody. The asterisks mark lymphatics containing immune cells. Bone lymphatics in *Osx-tTA;TetO-Vegfc* mice frequently contain immune cells. (D) Lymphatic vessel index values were determined for femurs stained using an anti-podoplanin antibody. Lymphatic vessel index values were significantly higher in vehicle-treated mice (179.9 ±11.51, *n*=5) than in rapamycin-treated mice (57.38±8.68, *n*=4). (E,F) Representative images of femur cross-sections stained with Hematoxylin and Eosin. (G) Cortical porosity values for vehicle (0.098±0.027, *n*=4) and rapamycin-treated mice (0.023±0.013, *n*=5). Data are mean±s.e.m. *P<0.05; ****P<0.0001; unpaired Student's *t*-test. Scale bar: 100 μm in B,C; XXXXX μm in E,F.

out to determine whether rapamycin could suppress the development of bone lymphatics in *Prox1-CreER^{T2};LSL-Pik3ca^{H1047R}* mice. Mice were injected with tamoxifen on P31, P33, P35, P39 and P42. We started to treat mice with vehicle or rapamycin on P70 (Fig. 10A). Our results in Fig. 7 show that *Prox1-CreER^{T2};LSL-Pik3ca^{H1047R}* mice do not have lymphatics in their bone on P70 (Fig. 7H). We collected femurs from mice on P91. We found that rapamycin-treated mice had significantly fewer bone lymphatics than vehicle-treated mice (Fig. 10B-D). Eight out of 10 vehicle-treated mice had bone lymphatics, whereas 0 out of 10 rapamycin-treated mice had bone lymphatics (*P*<0.001; Fisher's exact test). These results show that rapamycin can suppress the development of bone lymphatics in *Prox1-CreER^{T2};LSL-Pik3ca^{H1047R}* mice. We did not examine cortical porosity in *Prox1-CreER^{T2};LSL-Pik3ca^{H1047R}* mice because they develop a pleural effusion and die before they have significant bone involvement (Rodriguez-Laguna et al., 2019).

DISCUSSION
In 1955, Gorham and Stout reported that individuals with massive osteolysis can have ectopic lymphatics in their bone (Gorham and Stout, 1955). Since that groundbreaking observation, investigators

have been interested in the development of bone lymphatics and in identifying drugs that could inhibit the growth of lymphatics in bone. In the present study, we show that bLECs can arise from pre-existing LECs and that rapamycin can suppress the development of bone lymphatics.

LECs can arise from multiple different cell types. Lineage-tracing studies in mice have shown that LECs can arise from pre-existing LECs (Srinivasan et al., 2007), hemogenic endothelium (Stanczuk et al., 2015), blood endothelium (Martinez-Corral et al., 2015; Pichol-Thievend et al., 2018; Srinivasan et al., 2007) and from an unknown cellular source (Martinez-Corral et al., 2015). Bone marrow transplantation studies have shown that LECs can also develop from the hematopoietic lineage (Jiang et al., 2008). Additionally, tissue culture experiments have shown that macrophages and mesenchymal stem cells can express markers of lymphatic endothelium under certain culture conditions (Conrad et al., 2009; Hall et al., 2012). The cellular origin of bLECs was not previously known. We found that most of the bLECs in *Osx-tTA; TetO-Vegfc* and *Prox1-CreER^{T2};LSL-Pik3ca^{H1047R}* mice came from pre-existing Prox1-positive cells. However, not all of the bLECs in our mouse models expressed the lineage reporter. This could be due to an incomplete labeling of LECs in our animal models.
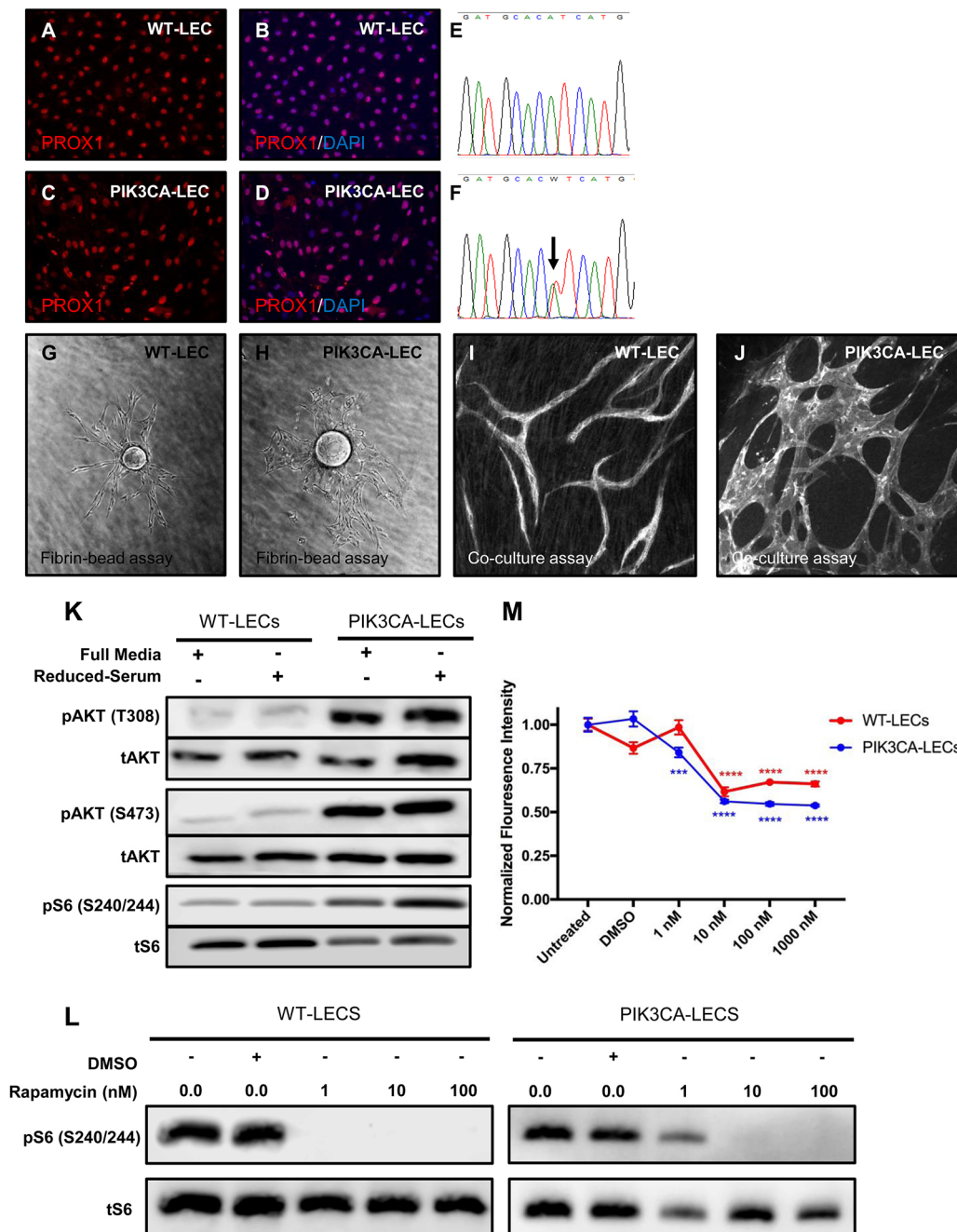
Fig. 9. PIK3CA-LECs form irregular vessels *in vitro* and rapamycin suppresses the growth of PIK3CA-LECs. (A-D) PROX1 immunostaining results for WT-LECs and PIK3CA-LECs. (E,F) Sanger sequencing results for WT-LECs and PIK3CA-LECs. PIK3CA-LECs have a somatic activating mutation in *PIK3CA* (arrow). (G,H) Fibrin-bead assay results for WT-LECs and PIK3CA-LECs. PIK3CA-LECs formed hyperplastic vessels. (I,J) Fibroblast co-culture assay results for WT-LECs and PIK3CA-LECs. PIK3CA-LECs formed hyperplastic vessels. (K) Immunoblot analysis with lysates from WT-LECs and PIK3CA-LECs. Lysates were made of cells cultured in full growth media or of cells cultured overnight in reduced-serum media. The levels of pAKT and pS6 were greater in PIK3CA-LECs than in WT-LECs. (L) Immunoblot analysis with lysates from cells treated with DMSO (vehicle) or rapamycin. Cells were treated with drug for 24 h. Rapamycin blocked mTORC1 signaling in WT-LECs and PIK3CA-LECs. (M) WT-LECs and PIK3CA-LECs were treated with DMSO or rapamycin (1, 10, 100 or 1000 nM) for 3 days. Cell viability was measured with a Cell-Titer Blue kit. Statistical significance was measured by ANOVA followed by a Dunnett's multiple comparisons test. Groups were compared to the untreated group. Data are mean±s.e.m. ***$P<0.001$; ****$P<0.0001$.

Alternatively, a small fraction of bLECs could come from a different cellular source. As more lymphatic endothelial progenitors are identified, additional lineage-tracing studies could be performed to determine whether other cell types give rise to bLECs.

We found that *Osx-tTA;TetO-Vegfc* mice that were exposed to doxycycline from E0.5 to P21 developed lymphatics in bone slower than mice that were exposed to doxycycline from E0.5 to E18.5. Tetracyclines, such as doxycycline, incorporate into mineralizing bone (Pautke et al., 2010). Because mice in the lineage-tracing study were exposed to doxycycline for a longer period of time, they could have accumulated more doxycycline in bone and required more time for the doxycycline to wash out. This could impact the expression of
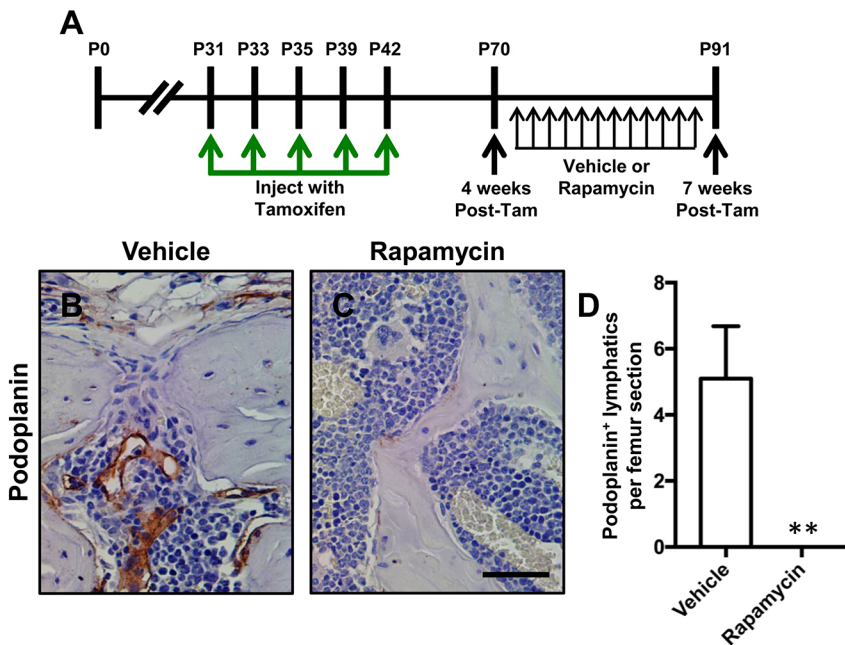
Fig. 10. Rapamycin suppresses the development of bone lymphatics in *Prox1-CreER^T2;LSL-Pik3ca^H1047R* mice. (A) Schematic showing when *Prox1-CreER^T2;LSL-Pik3ca^H1047R* mice were injected with tamoxifen (2 mg; i.p.). *Prox1-CreER^T2;LSL-Pik3ca^H1047R* mice were treated with vehicle or rapamycin (100 µg; 5 times/week; i.p.) from P70 to P91. (B,C) Representative images of femurs stained using an anti-podoplanin antibody. (D) Femurs from vehicle-treated mice (5.1±1.581, *n*=10) had significantly more lymphatics than femurs from rapamycin-treated mice (0±0, *n*=10). Data are mean±s.e.m. **P<0.01; unpaired Student's *t*-test. Scale bar: 50 µm.

VEGFC because we use a Tet-Off system to control the expression of VEGFC by bone cells. Another possible explanation is that bones in old mice might be more resistant to the development of bone lymphatics than bones in young mice.

We have previously analyzed the development of bone lymphatics in femurs from *Osx-tTA;TetO-Vegfc* mice (Hominick et al., 2018). However, we were not able to examine the initial stages of bone lymphatic development because we peeled away the periosseous muscle tissue from our samples. In the present study, we analyzed samples where we kept the periosseous tissue intact. This allowed us to gain further insight into the development of bone lymphatics. We found that lymphatics in control mice were restricted to the periosseous muscle tissue and they never crossed the periosteum. This raises the possibility that the periosteum protects bones from lymphatics. Additionally, the periosteum may express factors that prevent lymphatics from invading bone. Future *in vitro* and *in vivo* experiments could reveal whether the periosteum shields bones from lymphatics and inhibits lymphangiogenesis. In contrast to control mice, mutant mice had lymphatics that grew, breached the periosteum and then separated the periosteum from the underlying bone. The periosteum contains progenitor cells that differentiate into osteoblasts, which are cells that synthesize new bone (Dwek, 2010). Therefore, lymphatics in mutant mice might affect bone regeneration and repair by coming between the periosteum and bone. If this occurs in patients, it could contribute to the bone regeneration/repair defects observed in GLA and GSD.

Lymphatics need to pass through cortical bone before they colonize the marrow cavity. We have previously shown that LECs cannot directly degrade a matrix that mimics bone (Hominick et al., 2018). Therefore, a different cell type must clear the way for LECs. Osteoclasts are large multinucleated cells that resorb bone. We have previously reported that *Osx-tTA;TetO-Vegfc* mice have more osteoclasts than control mice (Hominick et al., 2018). In the present study, we have characterized the relationship between osteoclasts and lymphatics. We found that osteoclasts were closely associated with lymphatics invading bone. This raises the possibility that osteoclasts clear a path through bone for LECs. The close association between osteoclasts and lymphatics also raises the possibility that these two cell types

communicate with one another. Indeed, LECs have been reported to secrete M-CSF, a factor that promotes osteoclast development, and conditioned media from LECs has been shown to promote the formation of osteoclasts in a M-CSF-dependent manner (Wang et al., 2017). Conversely, osteoclasts have been reported to express VEGF-C (Zhang et al., 2008). The potential crosstalk between LECs and osteoclasts may serve an important role in the development of bone lymphatics. In the future, M-CSF could be conditionally deleted in LECs to determine whether its production by LECs promotes osteoclast formation *in vivo* and the invasion of bone by lymphatics.

We have previously reported that zoledronic acid (an osteoclast inhibitor) attenuated bone loss, but not the development of bone lymphatics, in *Osx-tTA;TetO-Vegfc* mice (Hominick et al., 2018). However, here we report that the invasion of bone by lymphatics is impaired in *Osx-tTA;TetO-Vegfc;Csf1^mut/mut* mice. One potential reason for this discrepancy is that the different approaches we used to inhibit osteoclasts differ in their ability to block osteoclast development and activity. Although zoledronic acid-treated mice had fewer osteoclasts than vehicle-treated mice (Hominick et al., 2018), they still had osteoclasts. In contrast, *Osx-tTA;TetO-Vegfc;Csf1^mut/mut* mice completely lacked osteoclasts. It is possible that the remaining osteoclasts in zoledronic acid-treated mice were sufficient to facilitate the development of bone lymphatics. It is also possible that the structural changes to bone in *Osx-tTA;TetO-Vegfc;Csf1^mut/mut* mice make the bone impenetrable to lymphatics or that the loss of other Csf1-dependent cells impairs the development of lymphatics in bone in *Osx-tTA;TetO-Vegfc;Csf1^mut/mut* mice. Presently, we are not able to distinguish between these possibilities.

In recent years, enthusiasm has grown for the FDA-approved drug rapamycin, because it has been found to have remarkable effects on the lymphatic system. Preclinical studies with mice that overexpress VEGFC in the lung (*CCSP-rtTA;TetO-Vegfc* mice) revealed that rapamycin can suppress VEGFC-induced lymphangiogenesis and partially reverse VEGFC-driven lymphangiectasia, and we have shown that rapamycin can suppress lymphangiogenesis in the skin of *Prox1-CreER^T2;LSL-Pik3ca^H1047R* mice (Baluk et al., 2017; Rodriguez-Laguna et al., 2019). In the clinic, rapamycin has been

found to be an effective treatment for lymphatic anomalies such as GLA and GSD (Adams et al., 2016; Cramer et al., 2016; Hammill et al., 2011; Ricci et al., 2019; Rodriguez-Laguna et al., 2019; Triana et al., 2017). A recent study examined the effect of rapamycin on disease response in 13 individuals with GLA and five individuals with GSD (Ricci et al., 2019). Bone disease did not progress in any of the individuals while they were on rapamycin (Ricci et al., 2019). Amazingly, it was reported that one patient with GLA had a complete resolution of their bone disease (Ricci et al., 2019). The evaluation of bones in individuals treated with rapamycin has been limited to imaging (MRI, CT and X-ray). This has made it difficult to determine the effect of rapamycin on bone lymphatics in individuals with GLA and GSD. By examining the histology of bones, we were able to show for the first time that rapamycin can inhibit the development of bone lymphatics. We also show that rapamycin can attenuate bone loss in *Osx-tTA;TetO-Vegfc* mice. One unresolved issue is whether rapamycin can induce the regression of lymphatics in bone. Unfortunately, the majority of our *Osx-tTA;TetO-Vegfc* and *Prox1-CreER^{T2};LSL-Pik3ca^{H1047R}* mice develop a pleural effusion and die shortly after they develop lymphatics in bone. This makes reversal studies with our models extremely challenging. Although we do not show that rapamycin can cause lymphatics in bone to regress, we believe that our preclinical findings provide further support for the testing of rapamycin as a treatment for individuals with GLA and GSD patients.

Taken together, our results shed light on the development of bone lymphatics, a process that has puzzled investigators since Gorham and Stout published their landmark paper over 60 years ago (Gorham and Stout, 1955). We also provide preclinical data showing that rapamycin, an emerging treatment for patients, can suppress the development of lymphatics in bone.

MATERIALS AND METHODS
Mice and genotyping
The animal experiments described in this article were carried out in accordance with an animal protocol approved by the Institutional Animal Care and Use Committee of UT Southwestern Medical Center. Mice were maintained in ventilated microisolator cages and were fed a standard diet *ad libitum*. Mice were provided igloos and nestlets as enrichment items. Both males and females were used in experiments. Littermates were used as controls for experiments. *TetO-Vegfc* (Lohela et al., 2008), *mT/mG* (Muzumdar et al., 2007), *Osx-tTA* (Rodda and McMahon, 2006), *Lyve1-Cre* (Pham et al., 2010), *LSL-Pik3ca^{H1047R}* (Adams et al., 2011) and *Prox1-CreER^{T2}* (Srinivasan et al., 2007) mice were genotyped as previously described (Dellinger et al., 2013; Hominick et al., 2018; Rodriguez-Laguna et al., 2019). *Csf1* mutant mice (Yoshida et al., 1990) were purchased from the Jackson Laboratory (stock number 000231) and were genotyped with the following primers: 5′-GCCT-AGGGTGTGATCGTCTC-3′; and 5′-TAAGGTTCAGGCTCGGTGAG-3′. PCR products were then sequenced to look for the presence of the causative genetic mutation (mutation=T insertion).

Doxycycline administration
We used the Tet-Off system to control the expression of VEGF-C by osterix-positive bone cells. Mice on normal drinking water express VEGF-C in bone, whereas mice on doxycycline water do not express VEGF-C in bone. Mice received water containing sucrose (5% w/v) and doxycycline (0.2 mg/ml or 1 mg/ml; Sigma-Aldrich, D9891), as indicated in the figure legends. Doxycycline water was replaced three times a week.

Preparation of tamoxifen and rapamycin
Tamoxifen (20 mg; Sigma, T5648) was dissolved in a mixture of ethanol (100 μl; Sigma, E7023) and sunflower oil (900 μl; Sigma, W530285). Mice received 100 μl of tamoxifen via an intraperitoneal injection. Rapamycin (Enzo, BML-A275-0025) was dissolved in ethanol to make a stock solution (50 mg/ml). The stock solution was then diluted to 1 mg/ml in a saline

solution that contained polyethylene glycol (5% w/v; Sigma, 88440) and Tween 80 (5% w/v; Sigma, P4780). Mice received 100 μg of rapamycin five times a week via an intraperitoneal injection.

Antibodies
The following primary antibodies were used for western blot analysis, immunohistochemistry or immunofluorescence staining: goat anti-Lyve1 (R&D Systems, AF2125, 1:250), chicken anti-GFP (Abcam, ab13970, 1:4000), hamster anti-podoplanin (Abcam, ab11936, 1:1000), rabbit anti-phospho-AKT T308 (Cell Signaling, 13038, 1:1000), rabbit anti-phospho-AKT S473 (Cell Signaling, 4060, 1:1000), rabbit anti-AKT (Cell Signaling, 4685, 1:1000), D2-40 (Abcam, ab52092, prediluted by company), rabbit anti-estrogen receptor (Abcam, ab27595, prediluted by company), rabbit anti-PROX1 (Cell Signaling, 14963, 1:100), rabbit anti-phospho-S6 S240/244 (Cell Signaling, 2D68F8, 1:1000) and rabbit anti-S6 (Cell Signaling, #2217, 1:1000).

Tissue fixation and decalcification
Mice were euthanized, perfused with PBS+heparin and then with 4% PFA. Bones were fixed overnight in 4% PFA and then decalcified for 2 weeks in 10% EDTA (pH 7.4). Bones were then processed and embedded by the histology core at UT Southwestern Medical Center.

Immunohistochemistry
Slides were deparaffinized and then rehydrated. A hydrogen peroxide/methanol solution was used to block endogenous peroxidase activity and TBST+20% Aquablock was used to block nonspecific binding of antibodies. Slides were incubated overnight with primary antibodies diluted in TBST+5% BSA. Slides were washed with TBST then incubated for 1 h with secondary antibodies diluted in TBST+5% BSA. Antibody binding was detected with an ImmPACT DAB Peroxidase Substrate Kit (Vector, SK-4105), which creates a brown color. Slides were then dipped in Hematoxylin (purple color) and dehydrated, and coverslips were mounted with CytoSeal (Thermoscientific, 8312-4). A similar protocol was used to stain liver sections, except antigen retrieval was performed with a 1× Tris-EDTA+10% glycerol solution and a modified secondary antibody (Vector, MP-7451) was used to detect the anti-ER primary antibody. We did not dip slides of liver in Hematoxylin so we could visualize nuclear ER staining.

Quantification of bone lymphatics
Lymphatic vessel index
Images were captured with a 40× objective and were analyzed in Image J. A 20-line by 26-line multipurpose test grid, with line length 9 μm, spacing 9 μm, total points 520 and total test area 180 μm×235 μm, was overlaid on images with tissue dimensions of 180 μm×235 μm. The total test area was 42,300 μm². We counted the number of times the gridlines intersected on lymphatics and in lymphatic lumens in the test area. We refer to this value as the 'Lymphatic Vessel Index'.

Lymphatics per femur section
To determine the number of lymphatics per femur section, we scanned an entire 5 μm longitudinal section of femur and counted the number of bone lymphatics in the section.

Assessment of GFP expression by lymphatics
Serial sections of bone were stained with antibodies against GFP and either Lyve1 or podoplanin. We captured images of the slides and then counted the number of GFP-positive and GFP-negative lymphatics.

Tartrate-resistant acid phosphatase (TRAP) staining and cortical porosity measurements
TRAP staining and cortical porosity measurements were performed as previously described (Hominick et al., 2018).

Cell culture
Primary adult human dermal LECs were purchased from LONZA (CC-2810). Cells were cultured on rat-tail collagen 1 (50 μg/ml) or fibronectin-coated

plasticware in EGM-2MV media (LONZA CC-3125). PIK3CA^{H1047L}-LECs were obtained from Dr Joyce Bischoff. These cells were isolated from a lymphatic malformation from a patient with a microcystic lymphatic malformation (Boscolo et al., 2015). Cells were found to be mycoplasma negative using a mycoplasma PCR detection kit (iNtRON, 25235).

Western blot analysis

Cells were scraped in lysis buffer [mPER (Thermo Scientific, 78501)+protease inhibitor (Thermo Scientific, 78425)+phosphatase inhibitors I and II (Sigma-Aldrich, P2850 and P5726)], spun for 10 min at 4°C and then supernatants were transferred to new tubes. Protein concentration was determined by performing a BCA assay. Equal amounts of protein were separated by SDS-PAGE then transferred to PVDF membranes. Membranes were blocked for 30 min at room temperature with either TBST+5% BSA or TBST+5% non-fat milk, incubated overnight at 4°C with phospho-specific primary antibodies, washed with TBST and then incubated for 1 h at room temperature with the appropriate HRP-conjugated secondary antibodies. Bound antibodies were detected with the SuperSignal West Pico PLUS Substrate detection system (Thermo Scientific, 34577). Membranes were re-blocked then re-probed with antibodies to detect the total level of target proteins.

In vitro lymphangiogenesis assays

A previously published protocol for HUVECs was used for the fibrin-bead assay with LECs (Nakatsu and Hughes, 2008). For fibroblast-LEC co-culture assays, primary human lung fibroblasts (PHLFs) were seeded in chambers of a four-well chamber slide. When the PHLFs were ~90% confluent, 50,000 LECs were added to the chambers. Cells were cultured for 6-7 days and media (EGM-2MV) were changed every other day. Chambers were washed with PBS and cells were fixed for 10 min with ice-cold methanol. Cells were washed with PBS then treated with PBS+20% Aquablock to block nonspecific binding of the primary antibody. Slides were incubated overnight with D2-40 (Abcam, ab52092), washed with PBS, then incubated with the appropriate secondary antibody diluted in PBS. Slides were then washed with PBS and coverslips were mounted with ProLong Gold plus DAPI (Invitrogen, P36931).

ICC staining of LECs

Cells were grown in the wells of a chamber slide. Old media were washed off with PBS. Cells were then fixed with ice-cold methanol for 10 min. Cells were then washed with PBS and blocked with PBS+20% Aquablock for 30 min. Cells were incubated overnight at 4°C with primary antibodies diluted in PBS+0.1% Tween20. Cells were washed and then incubated for 1 h with secondary antibodies diluted in PBS. Cells were washed again and coverslips were mounted with ProLong Gold plus DAPI.

Cell viability assay

LECs (5000 cells per well) were seeded into the wells of a Falcon Optilux Black/Clear bottom 96-well plate. The media were changed the next day and DMSO or rapamycin was added to the wells. Three days later, viability was assessed with either Cell Titer Blue (Promega, G8081) or MTS reagent.

Statistical analysis

Data were analyzed using GraphPad Prism statistical analysis software (Version 7.0). All results are expressed as mean±s.e.m. The number of mice in each group is indicated in the figure legends (*n*=number of mice). For experiments with two groups, unpaired Student's *t*-tests were performed to test means for significance. For experiments with more than two groups, differences were assessed by ANOVA followed by Dunnett's multiple comparisons test. Data were considered significant at $P<0.05$.

Supplementary information
Supplementary information available online at
http://dev.biologists.org/lookup/doi/10.1242/dev.184291.supplemental

Peer review history
The peer review history is available online at
https://dev.biologists.org/lookup/doi/10.1242/dev.184291.reviewer-comments.pdf

References

Adams, J. R., Xu, K., Liu, J. C., Agamez, N. M. R., Loch, A. J., Wong, R. G., Wang, W., Wright, K. L., Lane, T. F., Zacksenhaus, E. et al. (2011). Cooperation between Pik3ca and p53 mutations in mouse mammary tumor formation. *Cancer Res.* **71**, 2706-2717. doi:10.1158/0008-5472.CAN-10-0738

Adams, D. M., Trenor, C. C., III, Hammill, A. M., Vinks, A. A., Patel, M. N., Chaudry, G., Wentzel, M. S., Mobberley-Schuman, P. S., Campbell, L. M., Brookbank, C. et al. (2016). Efficacy and safety of sirolimus in the treatment of complicated vascular anomalies. *Pediatrics* **137**, 1-10. doi:10.1542/peds.2015-3257

Baluk, P., Yao, L.-C., Flores, J. C., Choi, D., Hong, Y.-K. and McDonald, D. M. (2017). Rapamycin reversal of VEGF-C-driven lymphatic anomalies in the respiratory tract. *JCI Insight* **2**, 90103. doi:10.1172/jci.insight.90103

Blesinger, H., Kaulfuß, S., Aung, T., Schwoch, S., Prantl, L., Rößler, J., Wilting, J. and Becker, J. (2018). PIK3CA mutations are specifically localized to lymphatic endothelial cells of lymphatic malformations. *PLoS ONE* **13**, e0200343. doi:10.1371/journal.pone.0200343

Boscolo, E., Coma, S., Luks, V. L., Greene, A. K., Klagsbrun, M., Warman, M. L. and Bischoff, J. (2015). AKT hyper-phosphorylation associated with PI3K mutations in lymphatic endothelial cells from a patient with lymphatic malformation. *Angiogenesis* **18**, 151-162. doi:10.1007/s10456-014-9453-2

Chen, J., Shi, Y., Regan, J., Karuppaiah, K., Ornitz, D. M. and Long, F. (2014). Osx-Cre targets multiple cell types besides osteoblast lineage in postnatal mice. *PLoS ONE* **9**, e85161. doi:10.1371/journal.pone.0085161

Conrad, C., Niess, H., Huss, R., Huber, S., von Luettichau, I., Nelson, P. J., Ott, H. C., Jauch, K.-W. and Bruns, C. J. (2009). Multipotent mesenchymal stem cells acquire a lymphendothelial phenotype and enhance lymphatic regeneration in vivo. *Circulation* **119**, 281-289. doi:10.1161/CIRCULATIONAHA.108.793208

Cramer, S. L., Wei, S., Merrow, A. C. and Pressey, J. G. (2016). Gorham-Stout disease successfully treated with sirolimus and zoledronic acid therapy. *J. Pediatr. Hematol. Oncol.* **38**, e129-e132. doi:10.1097/MPH.0000000000000514

Dai, X.-M., Ryan, G. R., Hapel, A. J., Dominguez, M. G., Russell, R. G., Kapp, S., Sylvestre, V. and Stanley, E. R. (2002). Targeted disruption of the mouse colony-stimulating factor 1 receptor gene results in osteopetrosis, mononuclear phagocyte deficiency, increased primitive progenitor cell frequencies, and reproductive defects. *Blood* **99**, 111-120. doi:10.1182/blood.V99.1.111

Dellinger, M. T., Meadows, S. M., Wynne, K., Cleaver, O. and Brekken, R. A. (2013). Vascular endothelial growth factor receptor-2 promotes the development of the lymphatic vasculature. *PLoS ONE* **8**, e74686. doi:10.1371/journal.pone.0074686

Dellinger, M. T., Garg, N. and Olsen, B. R. (2014). Viewpoints on vessels and vanishing bones in Gorham-Stout disease. *Bone* **63**, 47-52. doi:10.1016/j.bone.2014.02.011

Dwek, J. R. (2010). The periosteum: what is it, where is it, and what mimics it in its absence? *Skeletal Radiol.* **39**, 319-323. doi:10.1007/s00256-009-0849-9

Gorham, L. W. and Stout, A. P. (1955). Massive osteolysis (acute spontaneous absorption of bone, phantom bone, disappearing bone); its relation to hemangiomatosis. *J. Bone Joint Surg. Am.* **37-A**, 985-1004. doi:10.2106/00004623-195537050-00008

Hall, K. L., Volk-Draper, L. D., Flister, M. J. and Ran, S. (2012). New model of macrophage acquisition of the lymphatic endothelial phenotype. *PLoS ONE* **7**, e31794. doi:10.1371/journal.pone.0031794

Hammill, A. M., Wentzel, M. S., Gupta, A., Nelson, S., Lucky, A., Elluru, R., Dasgupta, R., Azizkhan, R. G. and Adams, D. M. (2011). Sirolimus for the

treatment of complicated vascular anomalies in children. *Pediatr. Blood Cancer* **57**, 1018-1024. doi:10.1002/pbc.23124

Hominick, D., Silva, A., Khurana, N., Liu, Y., Dechow, P. C., Feng, J. Q., Pytowski, B., Rutkowski, J. M., Alitalo, K. and Dellinger, M. T. (2018). VEGF-C promotes the development of lymphatics in bone and bone loss. *eLife* **7**, e34323. doi:10.7554/eLife.34323

Jiang, S., Bailey, A. S., Goldman, D. C., Swain, J. R., Wong, M. H., Streeter, P. R. and Fleming, W. H. (2008). Hematopoietic stem cells contribute to lymphatic endothelium. *PLoS ONE* **3**, e3812. doi:10.1371/journal.pone.0003812

Lala, S., Mulliken, J. B., Alomari, A. I., Fishman, S. J., Kozakewich, H. P. and Chaudry, G. (2013). Gorham-Stout disease and generalized lymphatic anomaly —clinical, radiologic, and histologic differentiation. *Skeletal Radiol.* **42**, 917-924. doi:10.1007/s00256-012-1565-4

Lee, L. K., Ghorbanian, Y., Wang, W., Wang, Y., Kim, Y. J., Weissman, I. L., Inlay, M. A. and Mikkola, H. K. A. (2016). LYVE1 marks the divergence of yolk sac definitive hemogenic endothelium from the primitive erythroid lineage. *Cell Rep.* **17**, 2286-2298. doi:10.1016/j.celrep.2016.10.080

Lohela, M., Heloterä, H., Haiko, P., Dumont, D. J. and Alitalo, K. (2008). Transgenic induction of vascular endothelial growth factor-C is strongly angiogenic in mouse embryos but leads to persistent lymphatic hyperplasia in adult tissues. *Am. J. Pathol.* **173**, 1891-1901. doi:10.2353/ajpath.2008.080378

Martinez-Corral, I., Ulvmar, M. H., Stanczuk, L., Tatin, F., Kizhatil, K., John, S. W. M., Alitalo, K., Ortega, S. and Makinen, T. (2015). Nonvenous origin of dermal lymphatic vasculature. *Circ. Res.* **116**, 1649-1654. doi:10.1161/CIRCRESAHA.116.306170

Muzumdar, M. D., Tasic, B., Miyamichi, K., Li, L. and Luo, L. (2007). A global double-fluorescent Cre reporter mouse. *Genesis* **45**, 593-605. doi:10.1002/dvg.20335

Nakatsu, M. N. and Hughes, C. C. W. (2008). An optimized three-dimensional in vitro model for the analysis of angiogenesis. *Methods Enzymol.* **443**, 65-82. doi:10.1016/S0076-6879(08)02004-1

Osborn, A. J., Dickie, P., Neilson, D. E., Glaser, K., Lynch, K. A., Gupta, A. and Dickie, B. H. (2015). Activating PIK3CA alleles and lymphangiogenic phenotype of lymphatic endothelial cells isolated from lymphatic malformations. *Hum. Mol. Genet.* **24**, 926-938. doi:10.1093/hmg/ddu505

Pautke, C., Vogt, S., Kreutzer, K., Haczek, C., Wexel, G., Kolk, A., Imhoff, A. B., Zitzelsberger, H., Milz, S. and Tischer, T. (2010). Characterization of eight different tetracyclines: advances in fluorescence bone labeling. *J. Anat.* **217**, 76-82. doi:10.1111/j.1469-7580.2010.01237.x

Pham, T. H. M., Baluk, P., Xu, Y., Grigorova, I., Bankovich, A. J., Pappu, R., Coughlin, S. R., McDonald, D. M., Schwab, S. R. and Cyster, J. G. (2010). Lymphatic endothelial cell sphingosine kinase activity is required for lymphocyte egress and lymphatic patterning. *J. Exp. Med.* **207**, 17-27. doi:10.1084/jem.20091619

Pichol-Thievend, C., Betterman, K. L., Liu, X., Ma, W., Skoczylas, R., Lesieur, E., Bos, F. L., Schulte, D., Schulte-Merker, S., Hogan, B. M. et al. (2018). A blood capillary plexus-derived population of progenitor cells contributes to genesis of the dermal lymphatic vasculature during embryonic development. *Development* **145**, dev160184. doi:10.1242/dev.160184

Ricci, K. W., Hammill, A. M., Mobberley-Schuman, P., Nelson, S. C., Blatt, J., Bender, J. L. G., McCuaig, C. C., Synakiewicz, A., Frieden, I. J. and Adams, D. M. (2019). Efficacy of systemic sirolimus in the treatment of generalized lymphatic anomaly and Gorham-Stout disease. *Pediatr. Blood Cancer* **66**, e27614. doi:10.1002/pbc.27614

Rodda, S. J. and McMahon, A. P. (2006). Distinct roles for Hedgehog and canonical Wnt signaling in specification, differentiation and maintenance of osteoblast progenitors. *Development* **133**, 3231-3244. doi:10.1242/dev.02480

Rodriguez-Laguna, L., Agra, N., Ibañez, K., Oliva-Molina, G., Gordo, G., Khurana, N., Hominick, D., Beato, M., Colmenero, I., Herranz, G. et al. (2019). Somatic activating mutations in PIK3CA cause generalized lymphatic anomaly. *J. Exp. Med.* **216**, 407-418. doi:10.1084/jem.20181353

Srinivasan, R. S., Dillard, M. E., Lagutin, O. V., Lin, F.-J., Tsai, S., Tsai, M.-J., Samokhvalov, I. M. and Oliver, G. (2007). Lineage tracing demonstrates the venous origin of the mammalian lymphatic vasculature. *Genes Dev.* **21**, 2422-2432. doi:10.1101/gad.1588407

Stanczuk, L., Martinez-Corral, I., Ulvmar, M. H., Zhang, Y., Laviña, B., Fruttiger, M., Adams, R. H., Saur, D., Betsholtz, C., Ortega, S. et al. (2015). cKit lineage hemogenic endothelium-derived cells contribute to mesenteric lymphatic vessels. *Cell Rep.* **10**, 1708-1721. doi:10.1016/j.celrep.2015.02.026

Triana, P., Dore, M., Cerezo, V. N., Cervantes, M., Sánchez, A. V., Ferrero, M. M., González, M. D. and Lopez-Gutierrez, J. C. (2017). Sirolimus in the treatment of vascular anomalies. *Eur. J. Pediatr. Surg.* **27**, 86-90. doi:10.1055/s-0036-1593383

Wang, W., Wang, H., Zhou, X., Li, X., Sun, W., Dellinger, M., Boyce, B. F. and Xing, L. (2017). Lymphatic endothelial cells produce M-CSF, causing massive bone loss in mice. *J. Bone Miner. Res.* **32**, 939-950. doi:10.1002/jbmr.3077

Yoshida, H., Hayashi, S.-I., Kunisada, T., Ogawa, M., Nishikawa, S.-I., Okamura, H., Sudo, T., Shultz, L. D. and Nishikawa, S. (1990). The murine mutation osteopetrosis is in the coding region of the macrophage colony stimulating factor gene. *Nature* **345**, 442-444. doi:10.1038/345442a0

Zhang, Q., Guo, R., Lu, Y., Zhao, L., Zhou, Q., Schwarz, E. M., Huang, J., Chen, D., Jin, Z.-G., Boyce, B. F. et al. (2008). VEGF-C, a lymphatic growth factor, is a RANKL target gene in osteoclasts that enhances osteoclastic bone resorption through an autocrine mechanism. *J. Biol. Chem.* **283**, 13491-13499. doi:10.1074/jbc.M708055200

DEVELOPMENT